Polymorphism and Crystal Morphology of Poly(ethylene oxide)−2-Methyl Resorcinol Supramolecular Complexes

L. Paternostre, P. Damman, and M. Dosière*

Laboratoire de Physico-Chimie des Polymères, Université de Mons-Hainaut, 20, Place du Parc B-7000, Mons, Belgium

Received June 23, 1998; Revised Manuscript Received November 2, 1998

ABSTRACT: The crystal structure and the morphology of poly(ethylene oxide) (PEO)−2-methyl resorcinol (MRES) supramolecular complexes are investigated by differential scanning calorimetry and wide-angle and small-angle X-ray scattering. Depending on the MRES content, two molecular complexes with different stoichiometries are observed. The first complex with a stoichiometry of 22 mol % MRES melts around 80 °C. This complex has a layered structure almost similar to the structure of the PEO−*p*-dihalogenobenzene intercalates. This complex results from the intercalation of MRES molecules between polymer layers. The second complex with a stoichiometry of 33 mol % MRES melts around 90 °C. Its crystal structure is dictated by the formation of a tight network of hydrogen bonds between host and guest molecules. In addition, depending on the experimental conditions, the growth of nonintegral-folded or integral-folded crystals of PEO−MRES complexes is observed from the small-angle X-ray diffraction curves. These different crystal morphologies are finally discussed in terms of the intermolecular interactions in these solid-state supramolecular assemblies.

Introduction

Poly(ethylene oxide) (PEO) is known to form molecular complexes with a large variety of organic and inorganic molecules.[1−9] The structure and the morphology of PEO−disubstituted aromatic molecule adducts (such as *p*-dihalogenobenzenes,[1] resorcinol,[5,7] *p*-nitrophenol,[6] and hydroquinone[7,9]) were investigated in our laboratory. The inclusion of polymer chains (PEO) in the crystal structure of molecular complexes hinders the formation of macroscopic single crystals suitable to perform a complete structure determination from X-ray diffraction data. The crystal structures of these systems must therefore be solved by combining different experimental techniques, i.e., X-ray diffraction of spherulite or uniaxially oriented samples, differential scanning calorimetry, and FTIR spectroscopy.

The phase diagram of the PEO/2-methyl resorcinol (MRES) system was previously reported by Belfiore[8] and exhibits two stable solid phases (polymorphs). However, their exact stoichiometries were not determined, and no attempt to solve their crystal structure was reported.

In this paper, we report on the formation of PEO−MRES supramolecular complexes in terms of the crystal structure and morphology. Crystal structures are proposed on the basis of stoichiometry and X-ray diffraction data. The lamellar crystals of ethylene oxide oligomers have an unique feature for macromolecules, the polymer chains are folded either an integral number of times (integral folded chain, IFC) or fully extended (extended chain, EC) inside the lamellar crystals, depending on the crystallization conditions. The relationships between the melting temperature, the lamellar thickness, and the crystallization temperature were investigated by several authors.[10] Recently, a transient state corresponding to crystals where polymer chains adopt a nonintegral folded conformation (NIFC) was reported by Cheng et al.[11] Time-resolved X-ray scattering measurements made during the first stages of crystallization show that these NIFC crystals spontaneously transform into more stable IFC or EC crystals. For PEO complexes, the crystal morphology is strongly affected by the nature of the aromatic guest molecules; e.g., the PEO−resorcinol complex grows as IFC or EC crystals[12] while the PEO−*p*-nitrophenol complex crystallizes with a NIFC morphology whatever the crystallization conditions.[12,13] In this paper, the morphology of both PEO−MRES crystal polymorphs was investigated by differential scanning calorimetry (DSC) and small-angle X-ray scattering (SAXS). The examination of the structure and the morphology of several PEO molecular complexes gives an insight into the formation of polymer supramolecular assemblies.

Experimental Section

Materials. Poly(ethylene oxide) (PEO) of low molecular weight ($M_w = 6000$) was a gift from Hoechst. High molecular weight PEO ($M_w = 5\ 000\ 000$) and MRES were purchased from Aldrich and used without purification. Spherulitic samples of PEO(6000)−MRES used for the polarizing optical microscopy investigations were crystallized in the form of thin films (≅ 20 μm) between glass slides. For the X-ray diffraction study, the spherulitic films of PEO(6000)−MRES molecular complex were mechanically supported by thin polypropylene films. Oriented films were also prepared by stretching at room temperature a quenched sample of molecular complex made of high molecular weight PEO ($M_w = 5\ 000\ 000$) and MRES.

Characterization. A differential scanning calorimeter (Pyris-1, Perkin-Elmer) was used for the determination of phase transitions. Sealed aluminum pans containing ≅5 mg of sample were used. The heating rate was 10 K/min. Optical observations were made on a DMR Leitz microscope. The nickel-filtered X-ray beam (Cu Kα radiation, $\lambda = 0.154\ 18$ nm) used for the diffraction experiments was produced by a rotating anode Rigaku Denki RU-200. Wide-angle X-ray diffraction patterns were recorded on Fuji image plates (IP) with 50 μm of lateral resolution. The IP reader was a BAS3000. As previously shown, the X-ray pattern obtained from the peripheral part of a large spherulite is a fiber pattern, the fiber axis being the radial growth axis of the spherulite. FTIR spectra were recorded on a Bruker IFS 113V Fourier transform infrared spectrometer: 32 co-added interferograms were scanned with a resolution of 2 cm^{-1}. The SAXS experiments and time-resolved WAXS intensity measurements were per-

10.1021/ma9809839 CCC: $18.00
Published on Web 12/12/1998

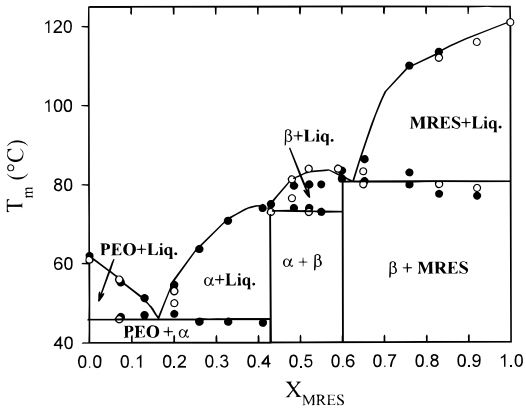

Figure 1. Phase diagram of the PEO−MRES system. Filled and open symbols correspond to the transition temperatures determined from DSC and wide-angle X-ray diffraction investigations, respectively.

formed at the D24 and D43 beam lines of the LURE-DCI synchrotron facility, respectively (Centre Universitaire de Paris-Sud, Orsay, France). The WAXD patterns were recorded during the heating of the sample with an Image plate as a detector on a modified Guinier-Lenne camera; a Molecular Dynamic reader was used. For SAXS measurements, a single bent germanium crystal with a (111) plane was used as a monochromator, the wavelength selected for the incident beam being 0.149 nm. The distance between the sample and the detector was 3 m. The SAXS intensity curves were recorded with a linear position sensitive detector. The draft intensity data were normalized with respect to the intensity of the incident beam and Lorentz corrected. The density correlation function $\gamma(d)$ was computed from the corrected SAXS intensity data with the following usual relation

$$\gamma(d) = \frac{\int_0^\infty I(s)s^2 \cos(2\pi sd)\, ds}{\int_0^\infty I(s)s^2\, ds}$$

where $s = 2(\sin\theta)/\lambda$ (2θ and λ being the diffraction angle and the wavelength of the X-ray beam, respectively).

The γ(d) functions were normalized to obtain $\gamma(0) = 1$. The linear degree of crystallinity (v^{lin}_c) was calculated from the long spacing (L) and the crystal thickness (L_c) obtained from the correlation function ($v^{lin}_c = L_c/L$).

Results

Phase Diagram of the PEO−MRES System. The phase diagram was determined from the transition temperatures obtained either by differential scanning calorimetry or by wide-angle X-ray diffraction when mixtures of PEO and MRES of various compositions are heated throughout their melting (122 °C). The DSC endothermic transitions associated with melting processes help to establish the phase diagram shown in Figure 1, which is essentially similar to that reported by Belfiore et al.[8] It results from the phase rule that observation of three different transitions occurring at a constant temperature (two eutectic and one eutectic−peritectic crossover phase transitions) is consistent with the formation of at least two molecular complexes. The transitions observed at 47, 78, and 81 °C, correspond to the melting of the PEO−α complex eutectic, that of the peritectic, or incongruent melting of the α complex and the β complex−MRES eutectic, respectively. The plot of the heats of transition vs the weight fraction of one component allows an accurate determination of the stoichiometry of the supramolecular complexes. For PEO−MRES, the heats of the PEO−α complex eutectic

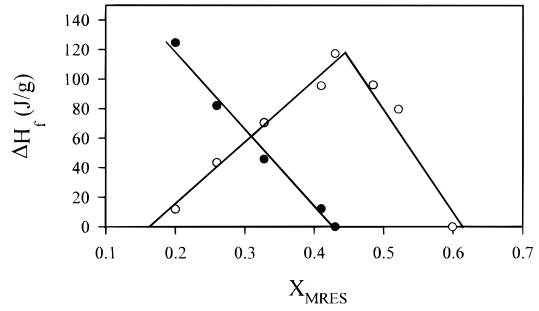

Figure 2. Heats of melting of the α complex (open symbols) and of the eutectic (filled symbols) vs the MRES weight fraction.

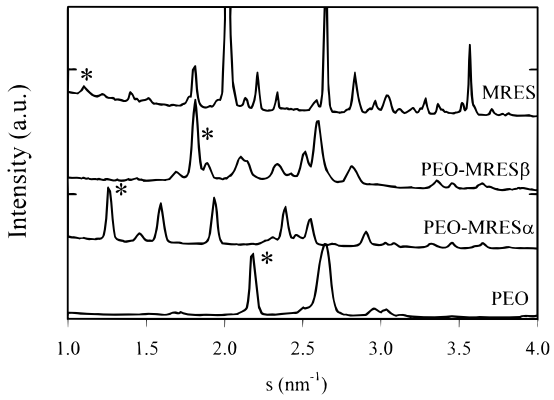

Figure 3. Powder WAXD curves of pure PEO, α complex, β complex, and pure MRES recorded at room temperature (as indicated). The s abscissa corresponds to the modulus of the scattering vector. The asterisks indicate what reflections are used to estimate the relative content of each crystalline phase during the melting of PEO−MRES mixtures (see the text for the indexation of these reflections).

transition and of the α complex melting vs the MRES content are plotted in Figure 2. A MRES stoichiometry of 44 wt % (22 mol %) for the α complex is estimated from the composition at which the eutectic heat vanishes and the melting heat of the complex is maximum. The stoichiometry of the β complex is determined from the composition at which the peritectic heat of the α complex vanishes (59 wt % or 33 mol % MRES). Thus, for α and β complexes, the stoichiometries determined by DSC correspond very nearly to two MRES molecules per seven EO monomers and one MRES molecule per two EO monomers, respectively.

To confirm the phase diagram established by DSC, the WAXD patterns of PEO−MRES mixtures with various MRES contents were recorded during their heating from room temperature to 90 °C. Figure 3 shows the powder diffraction curves obtained for pure PEO, pure MRES, PEO−MRES α complex ($X_{MRES} = 0.44$), and β complex ($X_{MRES} = 0.59$). A first examination of these intensity curves shows that α and β complexes actually correspond to new crystal forms. Some reflections, noticed by asterisks in Figure 3, are typical of the different crystalline phases. Their intensity was measured to estimate the relative proportion of the solid phases throughout the heating of the sample. The indexed reciprocal distances of these reflections are as follows:

$$\text{pure PEO: } s_{120} = 2.16 \text{ nm}^{-1}$$

$$\alpha \text{ complex: } s_{020} = 1.27 \text{ nm}^{-1}$$

β complex: $s_{210} = 1.80\ \text{nm}^{-1}$; $s_{200} = 1.90\ \text{nm}^{-1}$

MRES: $s = 1.10\ \text{nm}^{-1}$

Figure 4 shows the WAXD intensity recorded during the heating of samples with MRES contents of 0.07, 0.52, and 0.65, respectively. For the mixture with $X_{\text{MRES}} = 0.07$, the decrease in intensity of both PEO and α complex reflections indicates the melting of a eutectic followed by the melting of pure PEO. Similar observations were made for a 0.65 mixture containing both β complex and MRES crystals. For a MRES content equal to 0.52, an increase in intensity of the β complex reflections is observed, whereas those of α complex decrease. This observation confirms a peritectic reaction since the α complex spontaneously transforms into the β complex crystals. As shown later, this transformation can be related to the higher stability of the β complex with respect to the α one in terms of intermolecular interactions. The analysis of time-resolved WAXD curves recorded during the heating allows one not only to determine the different crystal species in the PEO−MRES sample but also to determine without ambiguity the nature of the transitions involved in the heating process.

Crystal Structure of the PEO−MRES α Complex. The crystal structure of the PEO−MRES α complex was determined from the study of oriented samples of PEO−MRES mixtures (22 mol % MRES) obtained, as indicated in the Experimental Section, either by low-temperature stretching of an amorphous sample made of high molecular weight PEO or by large spherulites ($M_w = 6000$) crystallized from the melt. The "fiber axis" of the drawn films and of the spherulites are the chain axis (*c* crystallographic parameter) and the radial growth direction, respectively. The diffraction pattern of a PEO−MRES α form stretched film is shown in Figure 5. From the Bragg spacings (d_{hkl}) and the angular position of the observed reflections, an orthorhombic unit cell with parameters $a = 1.04$ nm, $b = 1.59$ nm, and $c = 1.85$ nm can be determined (unit cell volume 3.059 nm^3). The indexation of the reflections observed in the X-ray pattern of a stretched sample is given in Table 1. Only one reflection condition was deduced from the indexation of the diffraction pattern: ($hk0$) with k even. By considering an orthorhombic symmetry, the $Pm2_1b$ space group can be proposed, a ($a - cb$) permutation of the $Pmc2_1$ space group (C_{2v}^2, No. 26 of the *International Tables of Crystallography*).[14] However, we should note that this group includes mirror planes which are usually not compatible with the packing of helices. Therefore, according to the few reflection conditions, the occurrence of a monoclinic cell, metrically orthorhombic, have also to be considered (e.g. $P2_1/a$ space group). The growth face of the spherulite, i.e., the plane with the highest growth rate, corresponds to the (020) crystallographic plane, which defines b^* as the fiber axis of the diffraction pattern. The observed layer lines in the stretched film (Figure 5) correspond to l values of 0, 2, 4, 5, 6, and 7. The Crick−Cochran−Vand rule was used to give a rough estimation of the structure factor of helices.[15] The following relation relates the value of l with the characteristic of the regular helix

$$l = tn + um$$

where u and t are the number of monomers and of turns by fiber period and n and m are integers.

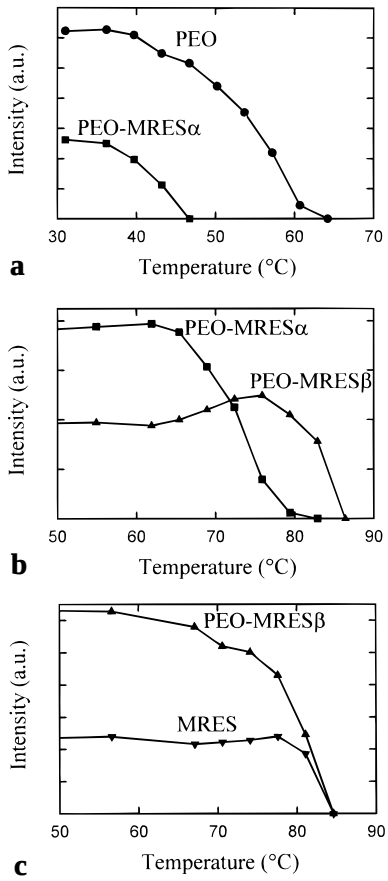

Figure 4. Variation of the diffracted intensity of the reflections characteristic of the different crystalline phases present in a PEO−MRES sample vs the temperature. The reflections used to estimate the relative content of each crystalline phase are described in the text. Parts a, b, and c refer to MRES contents (weight fraction) equal to 0.07, 0.52, and 0.65, respectively.

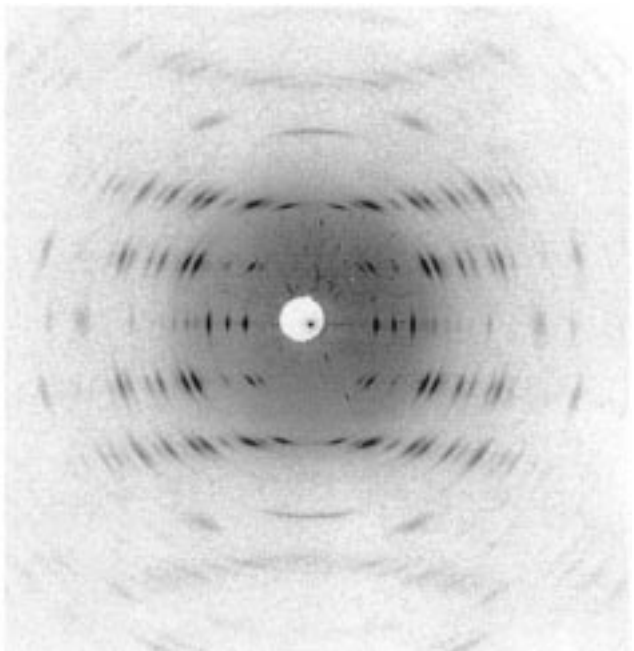

Figure 5. X-ray diffraction pattern of a stretched PEO−MRES α complex (0.44 MRES weight fraction). The drawn direction is vertical.

The average intensity of the layer lines observed in the X-ray pattern of a stretched film can be estimated

Table 1. Bragg Spacings and Miller Indexes of the Reflections Observed in the Diffraction Pattern of a Stretched PEO−MRES α Complex[a]

I[b]	d_{obs} (nm)	Miller indexes	d_{calc} (nm)	Δ (%)	I[b]	d_{obs} (nm)	Miller indexes	d_{calc} (nm)	Δ (%)
$l = 0$					w	0.288	(234)	0.289	0.4
s	0.791	(020)	0.793	0.3	w	0.276	(304)	0.277	0.4
m	0.630	(120)	0.630	0	s	0.272	(314)	0.273	0.4
s	0.518	(200)	0.519	0.2	w	0.260	(324)	0.261	0.4
w	0.434	(220)	0.434	0	w	0.253	(154)	0.253	0
vw	0.396	(040)	0.396	0	w	0.245	(334)	0.245	0
vw	0.370	(140)	0.370	0	w	0.233	(254)	0.233	0
		(230)	0.370		w	0.226	(404)	0.226	0
w	0.345	(300)	0.346	0.3	vw	0.224	(414)	0.224	0
w	0.315	(240)	0.315	0	vw	0.217	(424)	0.217	0
		(320)	0.317		$l = 5$				
w	0.260	(340)	0.260	0	vw	0.341	(115)	0.340	0.3
w	0.256	(160)	0.256	0	vw	0.303	(035)	0.303	0
		(410)	0.256		vw	0.252	(305)	0.252	0
$l = 2$					vw	0.241	(325)	0.240	0.4
s	0.690	(102)	0.690	0	w	0.234	(155)	0.234	0
s	0.633	(112)	0.633	0	w	0.219	(255)	0.218	0.2
m	0.522	(122)	0.520	0.2	vw	0.214	(345)	0.213	0.4
w	0.434	(212)	0.435	0.3	vw	0.205	(425)	0.205	0
s	0.419	(132)	0.419	0	vw	0.198	(355)	0.197	0.2
s	0.393	(222)	0.393	0	$l = 6$				
m	0.343	(232)	0.343	0	m	0.295	(106)	0.295	0
		(142)	0.343		m	0.265	(206)	0.265	0
m	0.324	(302)	0.324	0	m	0.261	(216)	0.261	0
m	0.298	(242)	0.298	0	vw	0.237	(236)	0.237	0
m	0.288	(152)	0.288	0			(146)	0.237	
w	0.276	(332)	0.276	0	vw	0.228	(316)	0.227	0.4
w	0.250	(342)	0.250	0	vw	0.220	(246)	0.220	0
		(402)	0.249		vw	0.203	(256)	0.203	0
vw	0.246	(162)	0.246	0	w	0.197	(416)	0.197	0
		(412)	0.246		$l = 7$				
w	0.228	(262)	0.228	0	m	0.250	(027)	0.250	0
$l = 4$					m	0.244	(127)	0.243	0.4
s	0.442	(014)	0.444	0.5	m	0.235	(207)	0.235	0
m	0.422	(104)	0.422	0			(037)	0.236	
s	0.408	(114)	0.408	0	m	0.226	(227)	0.225	0.4
m	0.399	(024)	0.399	0	w	0.220	(047)	0.220	0
m	0.371	(124)	0.373	0.5	$l = 8$				
m	0.345	(204)	0.345	0	w	0.210	(218)	0.209	0.5
w	0.337	(214)	0.337	0	vw	0.200	(048)	0.200	0
s	0.331	(134)	0.330	0.3	m	0.197	(238)	0.197	0

[a] The Bragg spacings are calculated on the basis of the proposed unit cell ($a = 1.04$ nm, $b = 1.59$ nm, $c = 1.85$ nm). [b] s, m, w, and vw refer to strong, medium, weak, and very weak reflections, respectively.

from the value of the integer n, corresponding to the order of the Bessel function involved in the computation of the structure factor. The smallest is the n value (0 or 1), the highest is the intensity of the layer line l. Solving the above equation for a 7_2 helix shows that intense layer lines correspond to l equal to 0, 2, 4, 5, 6, and 7. The 7_2 helix with a ttg conformation (the torsion angles are defined from the sequence C−O−C−C; t and g refer to trans and gauche angles, respectively) is similar to those reported for pure PEO in the monoclinic crystal form.[16] Moreover, this conformation is in very good agreement with the stoichiometry of seven EO monomer units for two MRES molecules, as deduced from the analysis of the phase diagram. We can therefore assume that, as previously reported for PEO-*p*-dihalogenobenzene complexes,[1] the MRES molecules are intercalated between adjacent PEO chains (Figure 6). The slight decrease observed for the average length of a monomer (0.264 nm instead of 0.278 nm for pure PEO) can be related to the formation of intermolecular interactions between host and guest molecules. The unit cell content is determined from the stoichiometry, the unit cell volume, and the measured density of the PEO−MRES α complex. Assuming 28 EO monomer units and eight MRES molecules in the cell, the calculated density

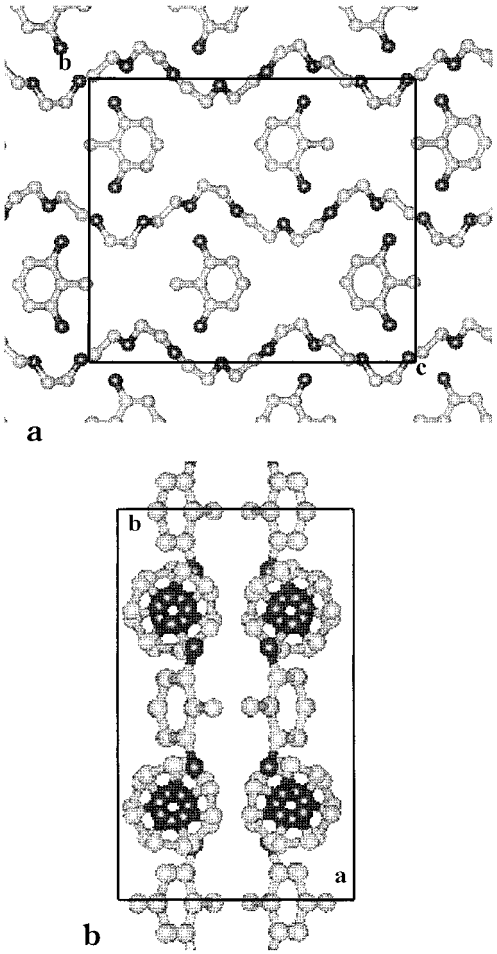

Figure 6. (a) Schematic view of the 7/2 helical conformation of PEO and disposition of the four MRES molecules intercalated between the polymer helices. (b) *ab* projection of the crystal structure of the α form of PEO−MRES complex (0.44 MRES weight fraction).

(1.210 g/cm^3) is in good agreement with the measured one (1.204 g/cm^3). The 28 EO units very likely distribute into four chains of seven monomers each. If the packing of left- and right-handed 7_2 helices is considered, the "corrugations" of these four chains create eight voids which can accommodate the 8 MRES molecules by an intercalation mechanism (Figure 6). The aromatic molecules are tilted by about 30° with respect to the chain axis, their orientation optimizing the formation of weak hydrogen bonds between the hydroxyl groups of the MRES molecules and some of the ether oxygen atoms of PEO. In addition, the close packing of two MRES molecules along the *c* axis generates a periodicity of 1.6 nm in agreement with the length of the *c* parameter (1.85 nm). Finally, a molecular model of the proposed crystal structure, viewed along the chain axis, is shown in Figure 6b. This model is in agreement with the most intense reflections observed in the X-ray diffraction patterns.

Crystal Structure of the PEO−MRES *β* Complex. Stretched and spherulitic samples of PEO−MRES *β* complex were prepared by the same methods described here above. Figure 7 shows the WAXD pattern recorded for a stretched film of *β* complex. The reflections observed in the diffraction pattern recorded for the stretched sample are indexed in Table 2. From these data, an orthorhombic unit cell is determined, the crystallographic parameters being $a = 1.11$ nm, $b = 1.86$

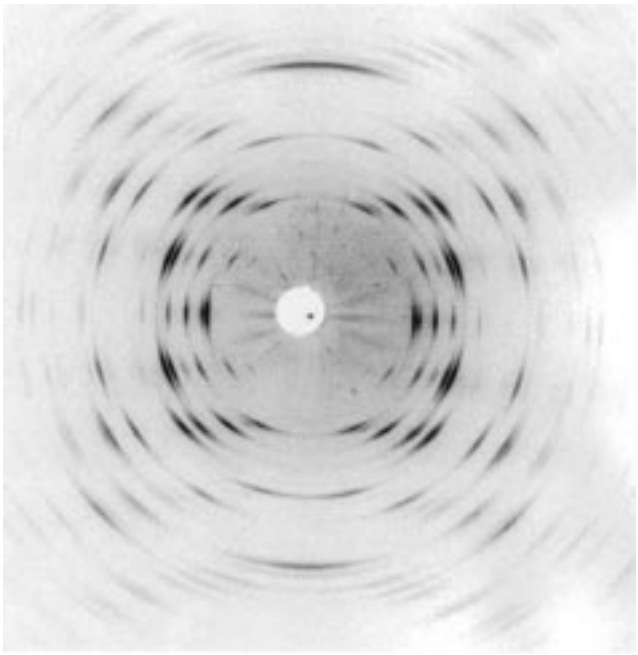

Figure 7. X-ray diffraction pattern of a stretched PEO−MRES β complex (0.60 MRES weight fraction). The drawn direction is vertical.

Table 2. Bragg Spacings and Miller Indexes of the Reflections Observed in the Diffraction Pattern of a Stretched PEO−MRES β Complex[a]

I	d_{obs} (nm)	Miller indexes	d_{calc} (nm)	Δ (%)	I	d_{obs} (nm)	Miller indexes	d_{calc} (nm)	Δ (%)
$l = 0$					s	0.377	(132)	0.379	0.5
s	0.551	(200)	0.552	0.2			(212)	0.375	
s	0.529	(210)	0.529	0	s	0.350	(042)	0.350	0
s	0.465	(040)	0.465	0	m	0.299	(242)	0.299	0
s	0.412	(230)	0.412	0			(152)	0.299	
m	0.356	(240)	0.355	0.3	m	0.272	(332)	0.272	0
vw	0.311	(060)	0.310	0.3	m	0.266	(252)	0.267	0.4
m	0.276	(400)	0.276	0	vw	0.260	(162)	0.260	0
w	0.253	(430)	0.252	0.4	w	0.244	(402)	0.244	0
w	0.240	(270)	0.239	0.4	w	0.240	(262)	0.240	0
w	0.232	(080)	0.232	0	$l = 3$				
vw	0.222	(450)	0.221	0.4	m	0.333	(113)	0.332	0.3
vw	0.215	(280)	0.214	0.4			(023)	0.331	
vw	0.206	(460)	0.206	0	w	0.296	(133)	0.296	0
$l = 1$					w	0.281	(043)	0.281	0
w	0.695	(021)	0.699	0.6	w	0.273	(143)	0.273	0
m	0.585	(121)	0.591	1.0	w	0.269	(233)	0.268	0.4
m	0.471	(211)	0.473	0.4	w	0.253	(313)	0.253	0
w	0.421	(041)	0.426	1.2	w	0.251	(243)	0.251	0
s	0.394	(141)	0.398	1.0	w	0.236	(333)	0.235	0.4
s	0.382	(231)	0.383	0.3	m	0.232	(253)	0.232	0
w	0.336	(241)	0.337	0.3	w	0.216	(413)	0.216	0
		(151)	0.335		w	0.204	(433)	0.205	0.5
vw	0.323	(321)	0.325	0.6	w	0.198	(273)	0.198	0
vw	0.302	(331)	0.303	0.3	w	0.187	(453)	0.187	0
w	0.294	(251)	0.296	0.7	$l = 4$				
m	0.285	(161)	0.287	0.7	m	0.257	(104)	0.258	0.4
w	0.276	(341)	0.278	0.7	w	0.249	(124)	0.248	0.4
vw	0.249	(171)	0.251	0.8	w	0.240	(204)	0.239	0.4
w	0.245	(431)	0.245	0	w	0.232	(224)	0.232	0
w	0.229	(361)	0.231	0.9	w	0.226	(144)	0.225	0.4
$l = 2$					m	0.213	(314)	0.214	0.5
m	0.480	(102)	0.478	0.4	vw	0.203	(334)	0.203	0
m	0.463	(112)	0.462	0.2	vw	0.201	(064)	0.201	0
		(022)	0.460		w	0.198	(164)	0.198	0
s	0.424	(122)	0.424	0	w				

[a] The Bragg spacings are calculated on the basis of the proposed unit cell (a = 1.11 nm, b = 1.86 nm, c = 1.06 nm). [b] s, m, w, vw refer to strong, medium, weak and very weak reflections, respectively.

nm, and c = 1.06 nm (unit cell volume 2.188 nm^3). The *Pbca* (D_{2h}^{15}, No. 61 in *International Tables of Crystallography*)[14] space group accounts for the following reflection conditions: (0kl) with k even, (h0l) with l even, and (hk0) with h even. The calculated density for a cell content of eight MRES molecules and 16 EO monomer units in agreement with the stoichiometry is 1.29 g/cm^3, a value very close to the experimental density measured by flotation (1.28 g/cm^3). The slight difference between these values can be attributed to the semicrystalline morphology of the polymer samples. In fact, the analysis of the correlation functions derived from SAXS intensity curves yields values of about 80−90% for the linear crystallinity.[12] To define the position and the orientation of the different molecules and macromolecules in the unit cell, the symmetry elements of the space group are considered. Since there are eight equivalent positions, the 16 monomers are assumed to distribute in four chains of four EO monomeric units. In contradistinction to the observations made for the PEO−MRES α complex, the fiber diffraction pattern of the drawn PEO−MRES β complex (Figure 7) displays all layer lines (l = 0, 1, 2, 3, or 4). No evidence of a 7_2 helical conformation is found. The length of a monomer (0.265 nm) is however consistent with a distorted 4_1 helical conformation already observed in PEO−RES[5] and PEO−HYD[9] molecular complexes. As expected from the stoichiometry, all the ether oxygen atoms form hydrogen bonds with the hydroxyl groups of the MRES molecules. Since the c glide plane symmetry is not supported by a 4_1 helix, the PEO chains have to be positioned on the 2-fold screw symmetry axes normal to the *ab* crystallographic plane at the following set of fractional coordinates (0,$^1/_4$), (0,$^3/_4$), ($^1/_2$,$^1/_4$) and ($^1/_2$,$^1/_4$) (Figure 8a). The orientation of the eight MRES molecules is determined by considering the formation of hydrogen bonds, a close packing of molecules, the symmetry elements, and the intensity of the equatorial reflections in the pattern of the drawn film ((200), (040), (210)). The proposed crystal structure is given in Figure 8b. As shown by Pimentel et al.[17] the shift observed for the ν_{OH} vibration can be roughly

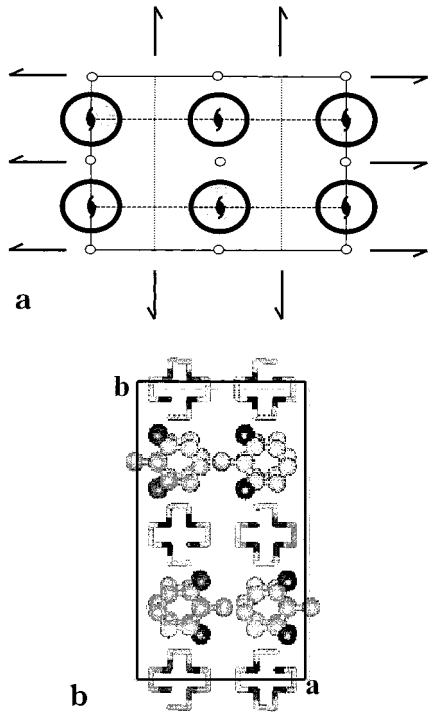

Figure 8. (a) Diagram of symmetry elements and orientation of the four PEO chains in the ab plane (filled and open symbols refer to left- and right-handed helices, respectively). (b) *ab* projection of the crystal structure of the β form of PEO−MRES complex (0.60 MRES weight fraction).

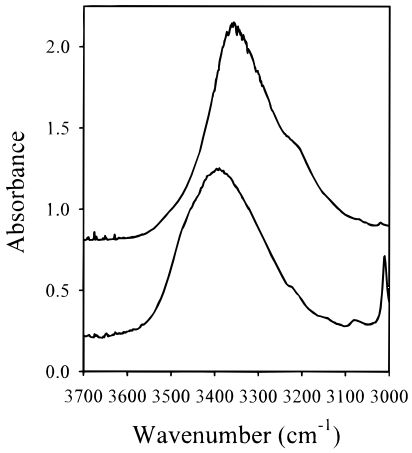

Figure 9. FTIR spectra (OH stretching region) of PEO−MRES α (lower curve) and β (upper curve) complexes.

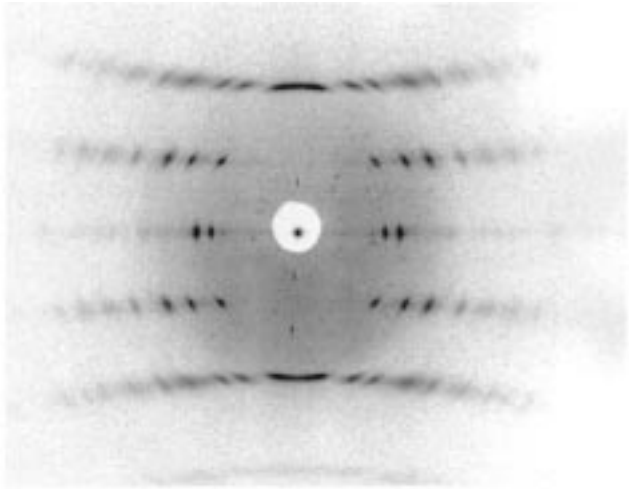

Figure 10. X-ray diffraction pattern of the stretched γ form of the PEO−MRES supramolecular complex.

related to the O−H···O distance. The frequency of the OH stretching IR band of both complexes (Figure 9) gives thus a rough estimate of the average strength of the hydrogen bonds. For the PEO−MRES complexes, the ν_{OH} frequency of the β form (3360 cm^{-1}) is slightly lower than that of the α form (3390 cm^{-1}). In addition, free OH groups are also observed in the FTIR spectra of the PEO−MRES α complex ($\nu_{OH\ free}$ = 3500 cm^{-1}).

Finally, it should be noted that PEO−MRES samples having the same stoichiometry of the β complex but nucleated at low temperature gives another crystal form which is called the γ form. As illustrated in Figure 10, the fiber pattern obtained from a stretched sample of PEO−MRES γ complex differs significantly from those of α and β complexes. From the observed reflections, a triclinic unit cell with parameters a = 1.75 nm, b = 1.51 nm, c = 0.91 nm, α = 91.3°, β = 93.5°, and γ = 66.0° was determined (unit cell volume = 2.196 nm^3). The γ form is metastable and transforms into the β form within a few days at room temperature. The kinetics of this transformation has not been investigated in more detail.

Crystal Morphology of the PEO−MRES α Form. Crystals of the PEO(6000)-MRES α complex were grown by isothermal crystallization from the melt. The Lorentz-corrected SAXS intensity curves recorded for samples crystallized at temperatures of 25, 40, 50, 60, and 70 °C are shown in Figure 11. The largest value of the long

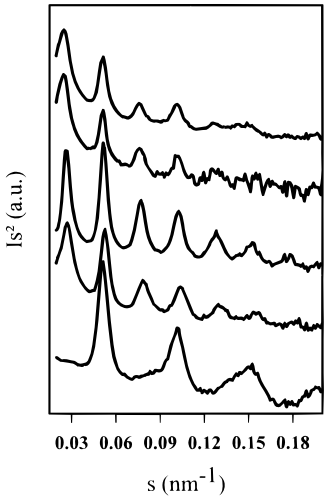

Figure 11. Selected Lorentz-corrected SAXS intensity curves for PEO−MRES α complex (0.44 MRES weight fraction) crystallized at 25, 40, 50, 60, and 70 °C (from bottom to top).

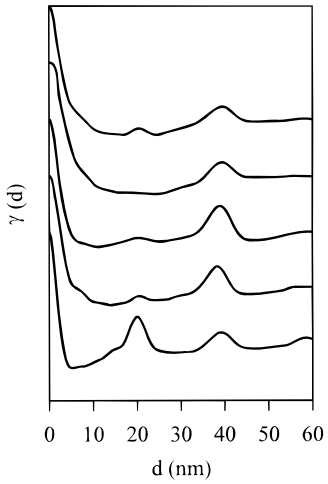

Figure 12. Correlation functions of the SAXS curves of PEO−MRES α complex given in Figure 11.

spacings determined by the position of the first Bragg peak in the SAXS curves is almost equal to the length of an extended chain of PEO (M_w = 6000). The different observed long spacings are constant and do not depend on the crystallization temperature. Note, however, that the relative intensities of the different Bragg peaks depend on the temperature. These observations clearly show that the PEO−MRES α complex forms crystals with the PEO chains folded an integral number of times. The other observed reflections are attributed to the successive diffraction orders of a periodicity corresponding to the thickness of one folded chain (1FC) or extended chain (EC) crystals. As previously reported for PEO−RES and PEO−HYD molecular complexes, the relative amounts of 1FC and EC crystals vary with the crystallization temperature. In the correlation functions of the SAXS curves shown in Figure 12, two peaks are observed at about 38 and 19 nm. In fact, these values correspond to the lamellar thickness of extended chain and one folded chain crystals, respectively. Therefore, their intensities are indicative of the relative fraction of EC and 1FC crystals in the sample. Figure 12 clearly shows that the amount of the EC crystals increases with the crystallization temperature, the folded crystals being however kinetically favored.

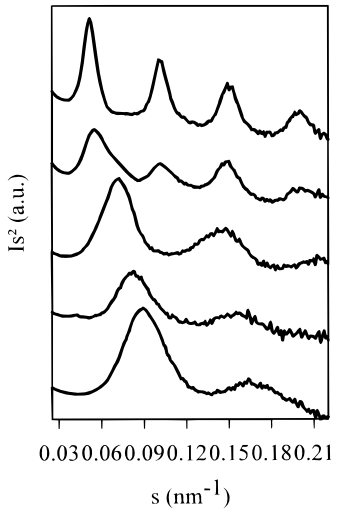

Figure 13. Selected Lorentz-corrected SAXS intensity curves for PEO−MRES β complex (0.60 MRES weight fraction) crystallized at 25, 40, 50, 60, and 70 °C (from bottom to top).

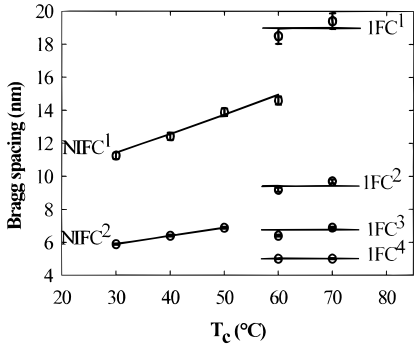

Figure 14. Plot of the peak position vs crystallization temperature for the different Bragg peaks observed in the SAXS intensity curves of the PEO−MRES β complex given in Figure 13.

Crystal Morphology of the PEO−MRES β Form. The β form of the PEO−MRES supramolecular complex is obtained by an increase of the MRES content (stoichiometry: two EO monomers for one MRES molecule). Figure 13 shows the SAXS intensity curves recorded for the PEO(6000)-MRES samples crystallized at 25, 40, 50, 60, and 70 °C. The long spacings are given in Figure 14. Contrariwise to all other complexes, two different modes of crystallization are observed for the PEO(6000)−MRES β complex (Figure 14). For low crystallization temperatures (i.e., T_c < 60 °C), the lamellar thickness corresponds to a NIFC morphology identical to the morphology observed for the PEO−PNP crystals. The position of the dominant SAXS peak continuously shifts toward small scattering vector(s). These shifts correspond to the thickening of the polymer crystals, the lamellar thickness increasing with the crystallization temperature. On the other hand, for high crystallization temperatures (i.e. $T_c \geq 60$ °C), the long spacings can be attributed to the diffraction orders corresponding to the thickness of one folded chain (1FC) crystals. The correlation functions computed from the SAXS intensity curves given in Figure 15 show that NIFC and 1FC crystallization domains overlap; i.e., the sample crystallized at 60 °C exhibits two periodicities at 15 nm (NIFC) and 19 nm (1FC). The analysis of the melting behavior of the PEO(6000)−MRES β complex by differential scanning calorimetry also illustrates the dual morphology of the β form of the PEO−MRES supramolecular complex. As shown in Figure 16, low-temperature endotherms are observed for crystallization temperatures lower than 60°C, their melting temperatures continuously increasing from 84 to 86 °C. The PEO−MRES samples crystallized at high temperature exhibit an endotherm at 91−92 °C, corresponding to 1FC and EC crystals. In addition, the equilibrium melting temperatures of PEO−MRES complexes were determined by plotting the melting temperatures vs the inverse of the lamellar thickness according to the Thomson-Gibbs relation

$$T_m = T_m^0\left(1 - \frac{2\sigma_e}{l\Delta H_m}\right)$$

where σ_e, l, and ΔH_m are the fold surface free energy, the lamellar thickness, and the melting enthalpy, respectively.

The α and β PEO−MRES complexes prepared from high molecular weight polymer (M_w = 200 000) were crystallized at various temperatures. The melting temperatures are plotted against $1/L$ in Figure 17. From the intercept at infinite crystal thickness ($1/L = 0$), equilibrium melting temperatures equal to 89 °C and 99 °C are determined for the α- and β-PEO−MRES complexes, respectively.

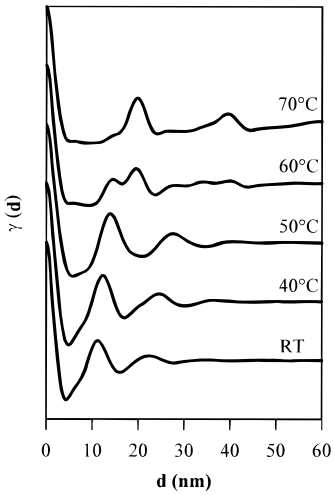

Figure 15. Correlation functions of the SAXS curves of the PEO−MRES β complex given in Figure 13.

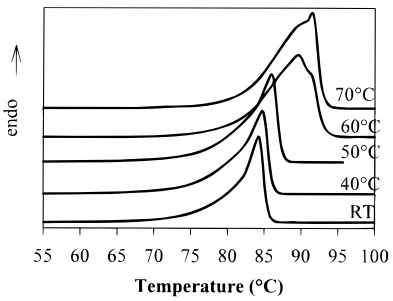

Figure 16. Melting curves of the PEO−MRES β complex crystallized at various temperatures. The thermograms were recorded by differential scanning calorimetry (heating rate 10 K/min).

Discussion

The formation of PEO supramolecular compounds can be discussed at two levels of description, the crystal

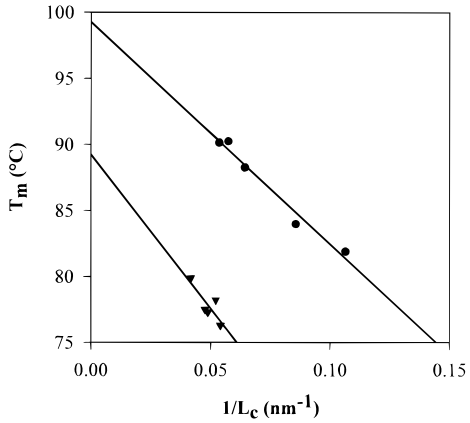

Figure 17. Plot of the melting temperatures of PEO−MRES crystals vs the reciprocal of the crystal thickness. Triangle and circle symbols correspond to α and β complexes, respectively.

structure and the crystal morphology. For PEO complexes involving weak intermolecular interactions, polymorphism is currently observed. Although the general features of the phase diagram are dictated by the most stable polymorph, other metastable crystal forms can be observed due to kinetic effects (rapid quenching, high supercooling, heterogeneous nucleation, ...). Regarding polymorphism, the PEO−MRES complex has an unusual behavior, i.e., two ***stable*** crystal forms are observed in the phase diagram. This peculiar behavior is assumed to reflect *the competition between the energy gained by the formation of hydrogen bonds associating host and guest molecules and the penalty due to departures of the chains from the conformation of minimum energy, these departures being required to accommodate the interacting molecules.* In the PEO−MRES α complex with a low MRES content, the PEO chains adopt a 7_2 helical conformation identical to that of pure crystalline PEO. The complexation mechanism corresponds thus to an ***intercalation*** of guest molecules between host polymer layers, following a pattern already observed for the structurally similar PEO−*p*-dihalogenobenzene intercalates.[1] As concerns the formation of hydrogen bonds in the PEO−MRES α form, all the oxygen atoms of the PEO macromolecules are not involved in interactions with MRES aromatic molecules, i.e., for seven ether oxygen atoms only four MRES hydroxyl groups are available. This looseness of the hydrogen bond network may be responsible for the lower melting temperature (T_m^0 = 89 °C) and the incongruent melting of the α complex which, when heated, spontaneously transforms into the β form.

For the PEO−MRES β complex, with a higher MRES content, the PEO chains adopt a distorted 4_1 conformation to accommodate the larger number or higher concentration of hydrogen bonds with MRES molecules; i.e., all four PEO oxygen atoms interact with the available four MRES hydroxyl groups. As previously shown, the most stable conformation of a PEO chain is the 7_2 helix.[18] The energy loss by the slight difference in conformation has to be compensated by the formation of intermolecular interactions (hydrogen bonds). The formation of an hydrogen bond network in the PEO−MRES β form is also supported by its melting temperature (T_m^0 = 99 °C), i.e., 10 °C higher than the melting temperature of the α form. In addition, we note that similar crystal structures were observed for the PEO−RES and the PEO−HYD supramolecular complexes involving a large number of hydrogen bonds. Their stoichiometry corresponds to two EO monomers for one aromatic molecule.

Finally, we may ask why polymorphism is observed for the PEO−MRES system whereas only one stable crystal form exists for the PEO−*p*-dihalogenobenzene, the PEO−RES, and the PEO−HYD molecular complexes? As a preliminary explanation of the polymorphism, we suggest that the methyl group of MRES molecules favors van der Waals and/or electrostatic interactions with the PEO chains and thus stabilize the low MRES content structure (α complex) much as for the *p*-dihalogenobenzene complexes. In addition, since the methyl group donates electron density on the aromatic ring, the ability of the MRES molecules to form hydrogen bond is slightly lower than for the resorcinol. This proposal requires however further experimental support, for example by analyzing the behavior of differently substituted resorcinol molecules. The morphology of PEO−MRES crystals, determined by SAXS and DSC investigations, also supports our proposal to explain the formation of the PEO complex. In fact, our analysis is based on the following two concepts: First, the crystal morphology reflects the intermolecular interactions. Second, the annealing of PEO crystals can be performed well below their melting temperature. The increase of the lamellar thickness due to the annealing process can be related to the high mobility of the PEO chains in the solid state. The measurement of relaxation times by NMR investigations has clearly demonstrated the influence of intermolecular interactions on the polymer mobility.[19] The occurrence of strong interactions obviously tends to decrease the chain mobility. The growth of PEO complex can be explained by the following scheme of crystallization, supported by time-resolved SAXS investigations. In the first stages of crystallization from the melt, unstable NIFC crystals grow with a lamellar thickness determined by the degree of supercooling. After their initial growth, these NIFC crystals are annealed, their lamellar thickness increasing with the annealing temperature. Finally, the formation of stable IFC or EC crystals is observed. The final morphology can thus be directly related to the strength of the intermolecular interactions. For a PEO complex involving strong hydrogen bonds, the NIFC morphology is maintained even after long annealing times at high temperatures.[12,13] For systems involving weak interactions, IFC or EC morphologies are observed when the samples are annealed during a short period of time. Depending on the MRES content, PEO−MRES complexes adopt different morphologies. In the crystals of the PEO−MRES α form, the polymer chains are either folded an integral number of times or fully extended, depending on the crystallization temperature. From the crystal structure (intercalates), the melting temperature (89 °C) and the stretching OH frequency (Figure 9), the interactions between host and guest molecules are assumed to be typical of weak van der Waals interactions. In fact, the occurrence of free and bonded OH groups can be deduced from the FTIR spectra ($\nu_{OH\ free}$ = 3500 cm^{-1}). However, an IR band at 3390 cm^{-1} typical of bonded OH is also observed for the PEO−MRES α complex, indicating the formation of weak hydrogen bonds between host and guest molecules. When these weak interactions are considered, the polymer chains possess enough mobility in the crystal to spontaneously rearrange even at low temperature.

For the PEO−MRES β form, a completely different morphology is observed. Stable NIFC crystals are observed for low crystallization temperatures. IFC crystals are observed only for crystallization temperatures higher than 60 °C. In fact, the crystal structure of the β form and the equilibrium melting temperature (99 °C) clearly show that strong hydrogen bonds are involved between host and guest molecules. Thus, at low crystallization temperatures (T_c < 60 °C), the intermolecular interactions hinder the displacement of PEO chain segments in the crystals, and neither IFC nor EC morphologies are observed. But, at high crystallization temperatures (T_c > 60 °C), the thermal energy becomes large enough to allow the displacement of the polymer chains in the crystals, the spontaneous evolution of crystals to the more stable IFC or EC crystals is therefore observed.

Conclusions

This study has demonstrated that depending on the MRES content, two molecular complexes are observed, having stoichiometry of 22 and 33 mol % MRES. For the low MRES content complexe, a layered orthorhombic structure was observed, the chain conformation being similar to the 7_2 helix of pure PEO. This complex actually results from the intercalation of the aromatic molecules between the polymer layers in the solid state. For the second molecular complex β (high MRES content), the crystal structure is orthorhombic. The unit cell contains four chains of four monomers and eight MRES molecules. The PEO chains adopt a 4_1 conformation. Contrariwise to the α complex, the structure of the β complex is mainly dictated by the formation of a hydrogen-bonding network between host and guest molecules.

Both these PEO molecular complexes exhibit a lamellar morphology typical of polymeric materials. As shown by SAXS and DSC investigations, the α complex crystallizes from the melt by forming either one folded or extended chain crystals. However, the β complex exhibits two different modes of growth. At low crystallization temperatures, the crystals correspond to a nonintegral-folded chain conformation similar to the morphology of PEO−*p*-nitrophenol. At high temperatures, integral-folded crystals are observed.

Finally, we note that the analysis and the refinement of these different crystal structures are actively in progress.

Acknowledgment. This work was supported by the Belgian National Funds for Scientific Research and the Science Program of the European Community for access to large scientific installations. P.D. is a Research Associate of the Belgian National Funds for Scientific Research. The authors thank Prof. P. Iannelli (Universita di Salerno, Salerno, Italy) and Dr B. Lotz (Institut Charles Sadron, Strasbourg, France) for helpful discussions of the manuscript and Dr. J. Doucet and C. Bourgaux for assistance on the D43 and D24 synchrotron beam lines (LURE, Université Paris-Sud, Orsay, France).

References and Notes

(1) Point, J. J.; Coutelier, C. *J. Polym. Sci., Polym. Phys. Ed.* **1985**, *23*, 231.
(2) Iwamoto, R.; Saito, Y.; Ishihara, H.; Tadokoro, H. *J. Polym. Sci., A2* **1968**, 1509.
(3) Yokoyama, M.; Ishihara, H.; Iwamoto, R.; Tadokoro, H. *Macromolecules* **1969**, *2*, 589.
(4) Tadokoro, H.; Yoshihara, T.; Chatani, Y.; Murahashi, S. *J. Polym. Sci, B* **1964**, *2*, 363
(5) Delaite, E.; Point, J. J.; Damman, P.; Dosière, M. *Macromolecules* **1992**, *25*, 4768.
(6) Point, J. J.; Damman, P. *Macromolecules* **1992**, *25*, 1184.
(7) Myasnikova, R. M.; Titova, E. F.; Obolonkova, E. S. *Polymer* **1980**, *21*, 403.
(8) Belfiore, L. A.; Veda, E. *Polymer* **1992**, *33*, 3833.
(9) Paternostre, L.; Damman, P.; Dosière, M. Submitted for publicaiton in *J. Polym. Sci., B: Polym. Phys. Ed.*
(10) (a) Kovacs, A. J.; Gonthier, A. *Kolloid. Z. Z. Polym.* **1972**, *250*, 530. (b) Arlie, J. P.; Spegt, P.; Skoulios, A. *Makromol. Chem.*, **1966**, *99*, 160. (c) Arlie, J. P.; Spegt, P.; Skoulios, A. *Makromol. Chem.* **1967**, *104*, 212.
(11) (a) Cheng, S. Z. D.; Zhang, A.; Chen, J.J. *J. Polym. Sci., Polym. Phys. Ed.* **1990**, *28*, 233. (b) Cheng, S. Z. D.; Chen, J. J.; Wu, S. X.; Zhang, A.; Yandrasatis, M. A.; Zhuo, R.; Quirk, R. P.; Habenschuss, A.; Zschack, P. R. In *Crystallization of Polymers*; Dosière, M., NATO ASI Series C 405; 1993, p 51.
(12) Paternostre, L.; Damman, P.; Dosière, M.; Bourgeaux, C. *Macromolecules* **1996**, *29*, 2046.
(13) Damman, P.; Point, J.-J. *Macromolecules* **1993**, *26*, 1722.
(14) *International Tables of Crystallography* Hahn, T., Ed., Kluwer: Dordrecht, The Netherlands, 1995; Vol. III.
(15) Cochran, W.; Crick, F. H. C.; Vand, V. *Acta Crystallogr.* **1952**, *5*, 581.
(16) Yoshihara, T.; Tadokoro, H.; Murahashi, S. *J. Chem. Phys.* **1964**, *41*, 2902.
(17) Pimentel, G. C.; Sederlom, C. H. *J. Chem. Phys.* **1956**, *24*, 639.
(18) Neyertz, S.; Brown, D.; Thomas, J. O. *J. Chem. Phys.* **1994**, *101*, 1064.
(19) Spevacek, J.; Paternostre, L.; Damman, P.; Draye, A.-C.; Dosière, M. *Macromolecules* **1998**, *31*, 3612.

MA9809839